ACS central science

Interfacial Superassembly of Mesoporous Titania Nanopillar-Arrays/Alumina Oxide Heterochannels for Light- and pH-Responsive Smart Ion Transport

Xin Zhang, Lei Xie, Shan Zhou, Hui Zeng, Jie Zeng, Tianyi Liu, Qirui Liang, Miao Yan, Yanjun He, Kang Liang, Lei Zhang, Pu Chen, Lei Jiang, and Biao Kong*

Cite This: *ACS Cent. Sci.* 2022, 8, 361−369

Read Online

ACCESS | Metrics & More | Article Recommendations | Supporting Information

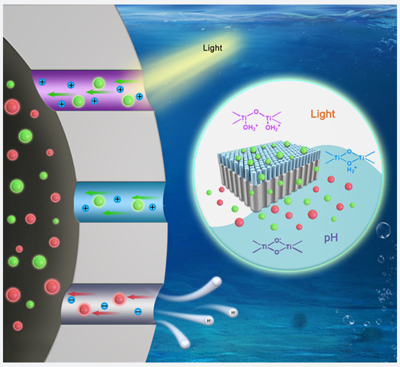

ABSTRACT: Stimuli-responsive nanochannels have attracted extensive attention in various fields owing to their precise regulation ability of ionic transportation. However, the poor controllability and functionality as well as responding to only one type of external stimulus still impede the development of the smart nanochannels. Here, we demonstrate a novel heterogeneous membrane composed of ordered mesoporous titania nanopillar-arrays/anodic aluminum oxide (MTI/AAO) using an interfacial superassembly strategy, which can achieve intelligent light and pH multimodulation ion transport. The MTI/AAO membranes are generated through the self-assembly of templates, followed by interfacial superassembly of micelles on AAO, and then the nanostructure and phase transformation of titania. The presence of the MTI layer with anatase crystal endows the heterogeneous membrane with an excellent light-responsive current density of 219.2 μA·cm^{-2}, which is much higher than that of a reported traditional light-responsive nanofluidic device. Furthermore, the MTI/AAO heterogeneous membranes with an asymmetric structure exhibit excellent rectification performance. Moreover, pH-regulated surface charge polarity leads to a reversal of current rectification polarity. This light and pH multiresponsive membrane realizes efficient, sensitive, and stable ion regulation, extending the traditional nanochannel from single modulation to smart multimodulation.

■ INTRODUCTION

Ion transport through cell membranes is precisely regulated by biological ion channels in organisms in response to external stimuli, which play a vital role in human physiological activities.[1] Inspired by biological ion channels, various artificial nanochannels with different functions emerge as a fascinating research field.[2−6] At present, various single-responsive artificial nanochannels that can respond to the external stimuli such as pH,[7−10] voltage,[11−13] temperature,[14−18] and light[19−25] have been reported. Thus, it is particularly important to develop novel nanochannels that can respond to multiple external stimuli. Success in this endeavor will give artificial nanochannels greater controllability and functionality, a significant step closer to biological ion channels. In particular, light- and pH-responsive ion channels have received wide and increasing attention due to their noninvasive external field control and intelligent ion response characteristics.[26−28] Therefore, it is significant to develop a nanofluidic device to make innovations in light and pH dual-functional ion channels.

Heterogeneous membranes composed of different materials are conducive to the construction of multi-stimulus-responsive nanochannels, because each component can be designed to respond to one external stimulus. A semiconducting membrane is considered as a potential candidate for the construction of photoresponsive ion channels due to its photoinduced surface charge and excellent photoregulated ion transport performance.[29,30] Titanium dioxide as a semiconducting material has received wide attention in recent years due to its excellent chemical stability and sensitive photoresponsive properties, which are conducive to mass diffusion and bring a sensitive and rapid response.[31] For example, Zhai et al. used Pt-nanoparticle-decorated TiO_2 nanotubes as photoresponsive ion channels, which generated a 385 nA·cm^{-2} of photocurrent under UV light with an irradiance of 8.4 mW·cm^{-2}.[32] An ordered mesoporous membrane composed of titania nanopillar-arrays has abundant and connected ion transport channels and not only provides three-dimensional (3D) ion transport channels but also increases the interaction interface between the ions and channel wall, which is expected to bring a higher responsive current. To our knowledge, there is no study that applies mesoporous titania nanopillar-arrays to light-responsive ion channels. In addition, anodic aluminum oxide (AAO) is an

Received: November 14, 2021
Published: February 14, 2022

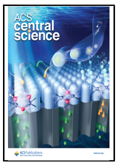

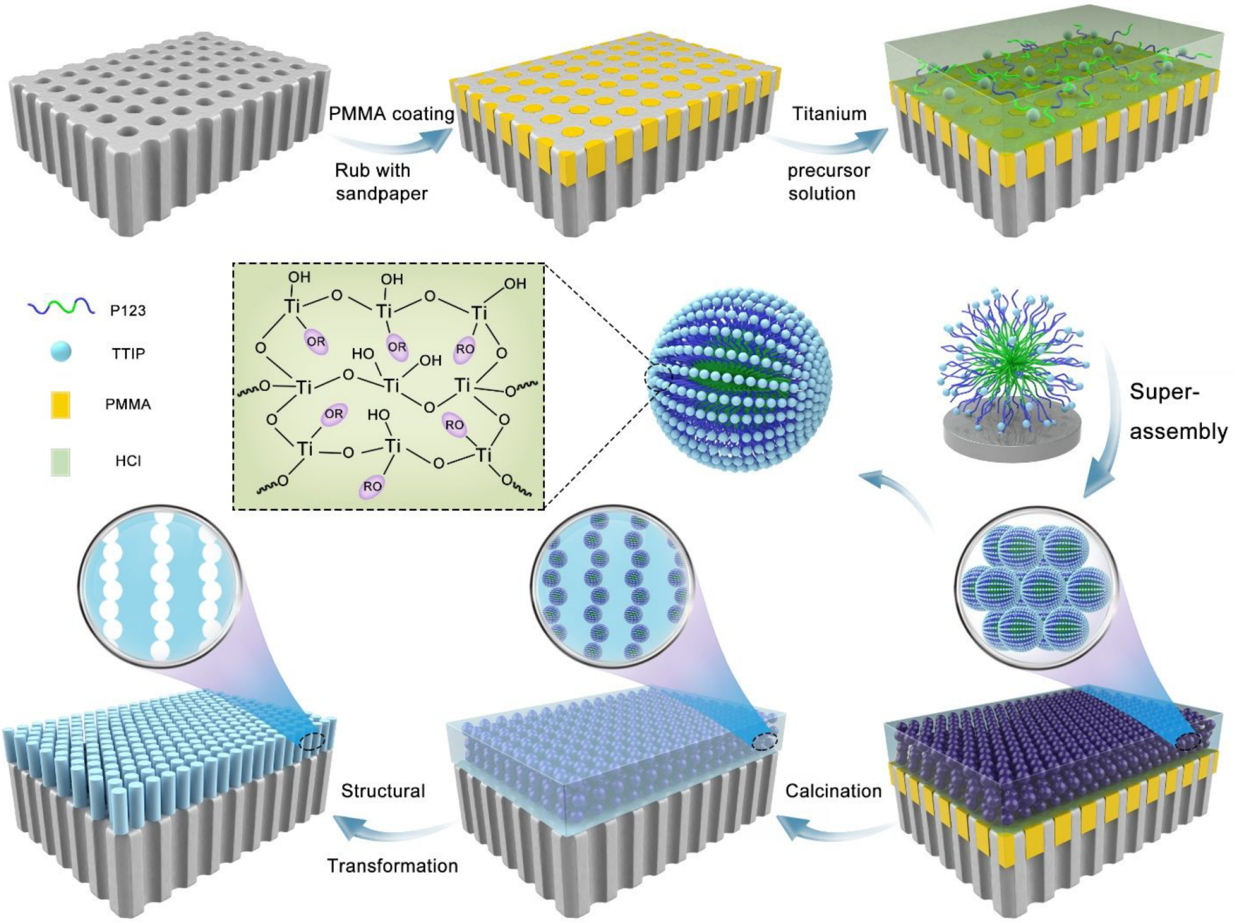

Figure 1. Schematic illustration of MTI undergoing structural transformation on the top surface of AAO nanochannels during the formation of heterogeneous MTI/AAO nanochannels by the interfacial superassembly method.

amphoteric compound, which not only shows different charge polarities at different pH values but also displays robust mechanical properties and good stability.[33] For instance, Zhou et al. employed AAO to prepare a pH-sensitive nanochannel for salinity gradient power generation.[34] Therefore, the integration of mesoporous titania and AAO is expected to construct light and pH dual-responsive nanochannels. Compared with a single external stimulus, the multi-stimulus-responsive nanochannels significantly improve the sensitivity of the ion channels and have stronger functionality and controllability.

Here, a unique structural transformation process is used to obtain a smooth MTI/AAO heterogeneous membrane with ordered structure and good stability. Then, a thin and smooth titania nanopillar-array membrane with a inverse mesoporous structure is successfully assembled on AAO (MTI/AAO) via an interfacial superassembly strategy. The MTI/AAO asymmetric heterogeneous membranes combine the properties of MTI and AAO, leading to the light-gated and the pH-adjustable ion transport properties as well as the diode-like rectified ion transport. Anatase titania with an ordered mesoporous structure and good crystallinity provides sensitive photoelectric response properties. The asymmetric chemical, electrostatic, and geometric composition endow the heterogeneous membranes with rectification performance, which can be regulated by light- and pH-induced surface charge. Furthermore, the abundant ion transport channels and high interaction interface provided by the MTI layer lead to a high light-responsive current density of 219.2 μA·cm^{-2}, which is much higher than that of the reported light-responsive nanofluidic device (Table S1). This multi-stimulus-responsive nanochannel combines the unique photoelectronic properties of mesoporous titania and the advantages of the the high mechanical properties of AAO membranes, exhibiting excellent stability, reversibility, as well as sensitivity, and is expected to be used in seawater desalination and biosensing fields.

■ RESULTS AND DISCUSSION

The MTI/AAO asymmetric heterogeneous membrane is constructed by an interfacial superassembly method with the assistance of hydrogen bonds and oxygen bridge bonds between MTI and AAO as shown in Figure 1.[33,35] To prevent the titania precursor solution from penetrating into the pores of AAO, poly(methyl methacrylate) PMMA was first spin-coated on the surface of AAO as a sacrificial layer (Supporting Information, Figure S1). The MTI precursor, which consists of a mixture of a titanium source (titanium tetraisopropoxide (TTIP)), hydrochloric acid, a template (Pluronic P123), and a solvent (alcohol), was coated on the AAO, and then, the ordered MTI was synthesized by evaporation-induced self-assembly (EISA) (Figure S2).[36] During the removal of the surfactant template by calcination, the MTI will undergo a structural transformation from a 3D hexagonal structure to mesoporous titanium dioxide pillar channels, which is expected to provide abundant 3D ion transport channels and interaction

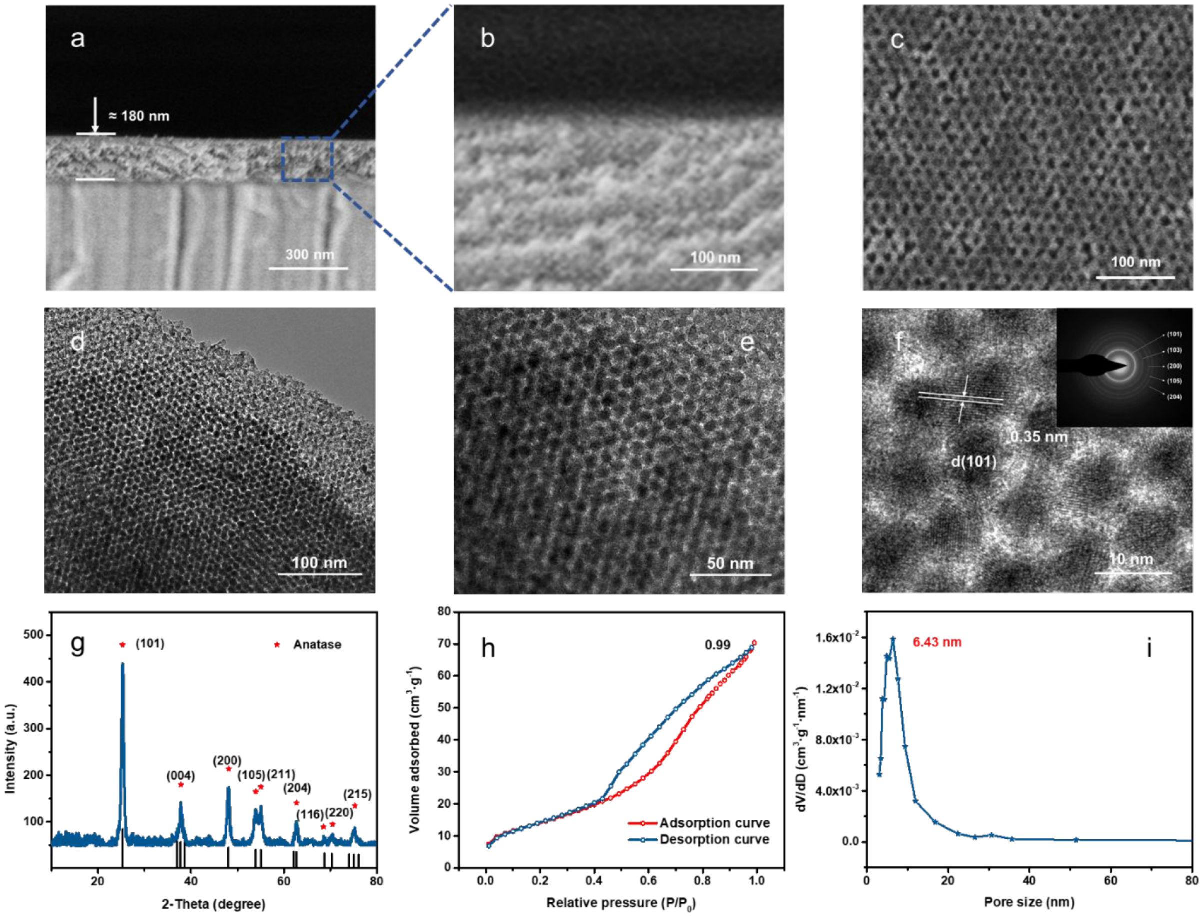

Figure 2. Characterization of the MTI/AAO heterogeneous membrane. (a,b) Cross-sectional and magnified SEM images of the MTI/AAO heterogeneous membrane. (c) Surface SEM image of the MTI/AAO heterogeneous membrane. (d−f) HRTEM images of ordered mesoporous TiO_2 at 97k, 195k, and 690k (the inset is the corresponding selected area electron diffraction pattern). (g) XRD pattern of the mesoporous TiO_2. (h) Nitrogen adsorption/desorption isotherms. (i) Corresponding pore size distribution of mesoporous TiO_2.

interfaces between the ions and channel wall, thus leading to superior ion transport.[37−39] TEM images of the MTI membrane at lower calcination temperatures demonstrate the formation of a 3D hexagonal structure with an ABAB stacking, and the appearance of elliptically shaped pores is caused by the contraction of the films (Figure S3).[40] In order to obtain the optimal structure, we prepared five different MTI membranes by calcination in the temperature range from 300 to 500 °C. The removal of the template P123 is confirmed by thermogravimetric (TG) analysis (Figure S4). The results of X-ray diffraction (XRD) indicate the crystallization of the amorphous titania framework to anatase, and the crystallinity becomes higher with the increase of temperature (Figure S5). The morphology of the MTI/AAO heterogeneous membrane was characterized by scanning electron microscopy (SEM) and transmission electron microscopy (TEM). When the temperature is lower than 400 °C, MTI can undergo structural transformation, resulting in poor mesospace order (Figures S6−S8). When the temperature is higher, the mesoporous structure collapses due to the crystallization of titanium dioxide (Figure S9).[41] The samples annealed at 400 °C represent the best balance between mesostructure and crystallinity and were employed in the following studies.

The cross-sectional SEM imagines show that the MTI/AAO asymmetric heterogeneous membrane is composed of a 180 nm thick layer of an ordered mesoporous titania layer atop an AAO substrate (Figure 2a,b). The surface SEM image verified that MTI/AAO membrane has no defects and exhibits a highly regular honeycomb arrangement over the entire top surface (Figures 2c and S10). The ordered mesoporous channels can be further verified by TEM (Figures 2d,e and S11). In addition, high-resolution transmission electron microscope (HRTEM) images (Figure 2f) and the corresponding selected area electron diffraction pattern shown in the inset indicate that the crystal lattice is indexed to anatase. The XRD diffraction peaks of the calcined membrane can be perfectly matched to the anatase phase, further demonstrating the formation of the anatase phase (Figure 2g).[42] The nitrogen adsorption desorption isotherms of MTI depict the representative type IV curve featuring a hysteresis loop, which further confirms the uniform mesoporous materials (Figure 2h).[43] The pore size of MTI calculated by the Barrett−Joyner−Halenda (BJH) model is as large as ∼6.43 nm (Figure 2i). The corresponding UV−vis absorption spectrum and the FT-IR spectrum of MTI are shown in Figures S12 and S13. The UV absorption intensity of MTI decreases sequentially at the wavelengths of 350, 365, and 380 nm, representing a controllable light-gated effect that can be achieved by the above wavelengths. In addition, the FT-IR spectrum indicates that there are abundant oxygen-containing functional groups in the MTI layer, which could supply abundant interaction interfaces between the ions and the channel wall.

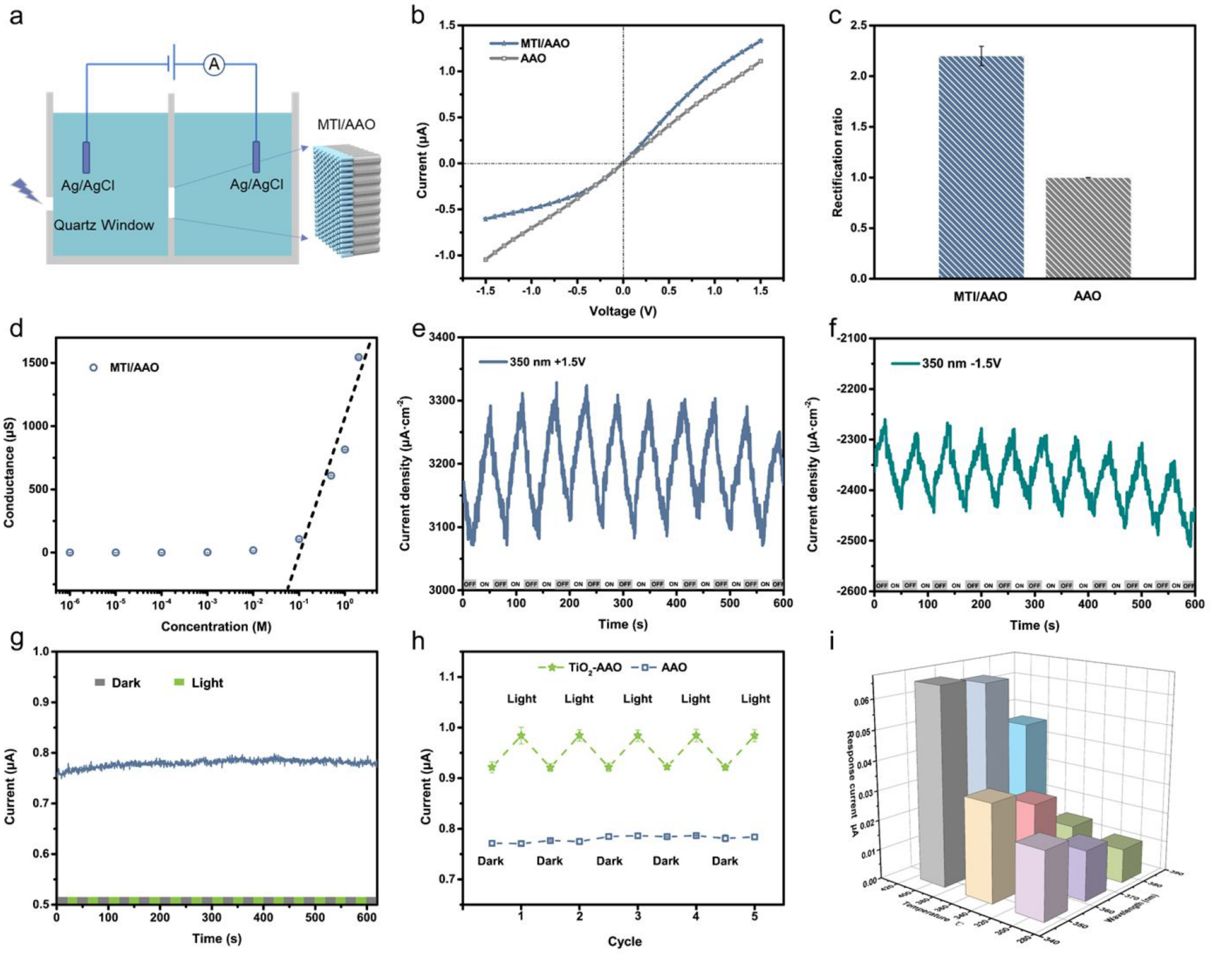

Figure 3. (a) Schematic diagram of the double-chamber electrochemical cell with a quartz window for the measurements of ionic current. (b) Current−voltage (I−V) curves of pure AAO and MTI/AAO heterogeneous membranes measured in 1 mM KCl solution of pH = 5 in the dark. (c) Rectification ratio of MTI/AAO and pure AAO. (d) The ionic conductance of a heterogeneous membrane under different KCl concentrations in the dark. (e,f) Current density−time curves of an MTI/AAO heterogeneous membrane at +1.5 and −1.5 V under alternating illumination. (g) Current−time (I−T) curves of a pure AAO membrane at +1.5 V under a 350 nm UV wavelength. (h) Reversible and stable switching ability of the heterogeneous MTI/AAO and pure AAO nanochannels at +1.5 V for variation of illumination. (i) Responsive current of MTI/AAO heterogeneous membranes prepared at different calcination temperatures under different wavelengths of UV light at +1.5 V. Error bars represent the s.d.

As shown in Figure 3a, the MTI/AAO heterogeneous membrane was installed between two electrochemical chambers filled with KCl solutions. The UV light was irradiated to the TiO_2 side through a quartz window, and a picoammeter was used to measure the ion current and conductance. Figure 3b illustrates the I−V curves of pure AAO and MTI/AAO heterogeneous membranes. Pure AAO has a linear I−V curve due to its symmetrical chemical composition. For the MTI/AAO heterogeneous membrane, a nonlinear I−V curve was observed with an ionic rectification ratio of approximately 2.2 (Figure 3c). The rectification ratio was defined as the current at +1.5 V $|I^+|$ divided by the absolute value of current at −1.5 V $|I^-|$. The ionic conductance of the MTI/AAO heterogeneous membrane was measured under different KCl concentrations. As shown in Figure 3d, the ionic conductance deviates significantly from the bulk value (dotted line) when the electrolyte concentration is less than 0.1 M, demonstrating that the ion transport is fully governed by the surface charge.[44] Beyond that, the ion conductance under the irradiation shows a trend similar to that in the dark (Figure S14). Meanwhile, the ionic conductance under irradiation is higher than that in the dark. Figure 3e,f shows the temporal photocurrent of the MTI/AAO heterogeneous membrane under voltages of +1.5 and −1.5 V, respectively. The corresponding photoresponsive current density at +1.5 V was approximately 219.2 μA·cm^{-2}. The state of the ion channel under light is defined as "on", and the state in the dark is defined as "off". The photoresponsive current density can also be improved by increasing the illumination intensity or prolonging the illumination time, and the transmembrane potential also has a similar trend under a different illumination intensity (Figures S15 and S16). In addition, we tested the current density generated by water decomposition under the same conditions, which can be ignored compared with the strong photoresponsive current density (Figure S17). The MTI/AAO can perform multiple reversible switching of on and off states under alternate light conditions, but the pure AAO film did not show light-responsive properties (Figure 3g,h). The responsive current of MTI/AAO shows an obvious relationship with the light wavelength and calcination temperature. Under the different wavelengths of UV light irradiation with the same power density (3.5 mW·cm^{-2}), the responsive current at 350 nm is the largest and decreases sequentially at 365 and 380 nm, which is consistent with the UV absorbance

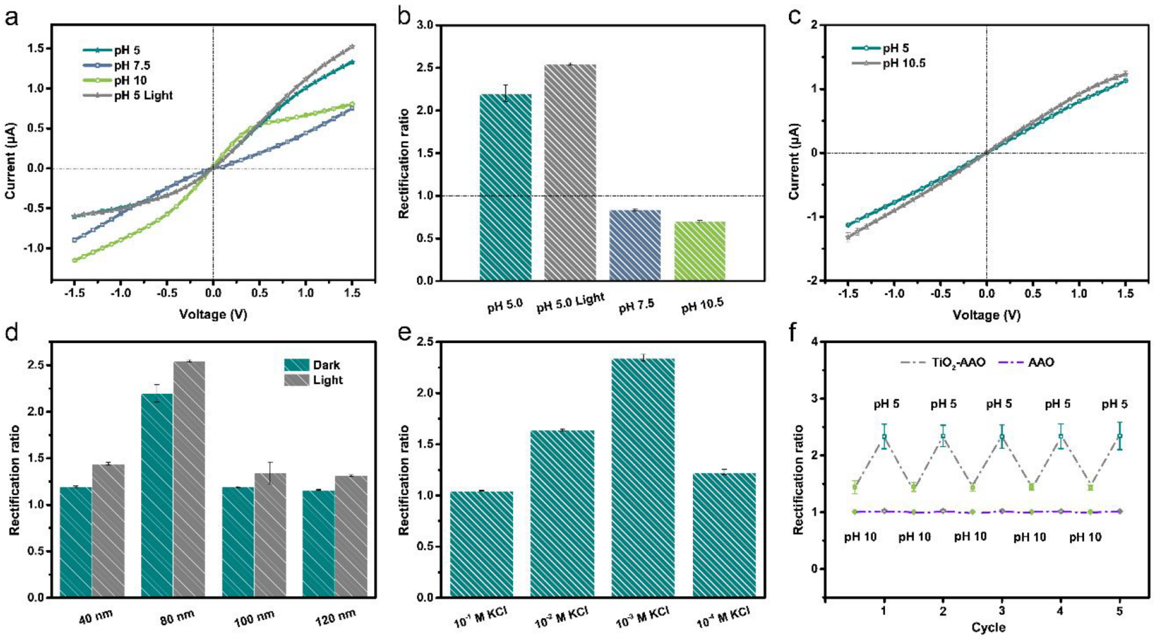

Figure 4. (a) *I*−*V* curves of MTI/AAO heterogeneous membranes measured in 1 × 10^{-3} M KCl with different pH values. (b) The ionic current rectification ratio of MTI/AAO heterogeneous nanochannels under different pH conditions. (c) *I*−*V* curves of the pure AAO membrane measured in 1 × 10^{-3} M KCl with different pH values. (d) The ionic current rectification ratio and *I*−*V* curves of MTI/AAO with different apertures before and after illumination. (e) The calculated rectification ratios of MTI/AAO heterogeneous nanochannels in KCl electrolyte with different concentrations under a pH value of 5. (f) Reversible and stable switching abilities of the heterogeneous MTI/AAO and pure AAO nanochannels at +1.5 V for the variation of pH values. Error bars represent the s.d.

of MTI/AAO. In addition, MTI has a higher responsive current at a higher calcination temperature, which is attributed to the enhancement of the crystallinity (Figures 3I and S18).[45]

In addition to the inherent optical properties of titanium dioxide, as a multi-stimulus-responsive nanochannel, MTI-AAO also exhibits a pH-regulated ion flux due to the different charge distributions of the heterogeneous nanochannel under different pH conditions. As the isoelectric point of titanium dioxide is 6.6 and the isoelectric point of AAO is 8.5, electrolytes at pH values of 5, 7.5, and 10.5 are chosen in the study of ionic transport properties (Figure S19).[46] At these three pH values, the heterogeneous channels are positively, partially positive, and completely negative charged, respectively. This is conducive to fully study the influence of pH on the ion transport in asymmetric heterogeneous membranes. According to Figure 4a, nanochannels exhibited different rectification behaviors at these three different pH values. As shown in Figure 4b, we calculated the ion rectification ratio at different pH conditions and under illumination. When pH = 5, the rectification ratio is greater than 1 under both light and darkness, while when pH = 7.5 or 10.5, the rectification ratio is reversed. In contrast, an unmodified AAO still didn't exhibit a rectifying performance under different pH conditions due to its symmetrical structure (Figure 4c). The heterogeneous membranes calcined at 350 °C show a similar rectification trend (Figure S20). In addition, the rectification ratio with different AAO apertures under illumination is slightly larger than that in the dark, up to 2.55 (Figures 4d and S21). Furthermore, we test the effect of electrolyte concentration on the ion current rectification. As shown in Figure 4e, as the KCl concentration increases, the rectification ratio first increases and then decreases, reaching a maximum at 10^{-3} M. The different rectification ratio is attributed to the variation in the thickness of the electric double layer (EDL). The thickness of the EDL gradually decreases as the electrolyte concentration increases.[47] For a high electrolyte concentration, the EDL cannot effectively overlap, thereby weakening the ion transport governed by the surface charge. When the electrolyte concentration is 1 mM, the rectification ratio reaches its maximum value, which is attributable to the thickness of the EDL equivalent to the pore size of the MTI[34,48] (Figure S22). The ion rectification cycles at different pH values (Figure 4f) confirm that the rectification characteristics of the heterogeneous channel exhibit excellent reversibility and stability.

To elucidate the mechanism of ion rectification properties, a theoretical simulation based on the Poisson and Nernst−Planck (PNP) equations was implemented to clarify the features within the multi-stimulus-responsive nanochannels. The simplified model consists of 600 nm long AAO nanochannels with a width of 80 nm and 150 nm long MTI nanochannels with a width of 6.4 nm (Figure S23). Figure 5a shows two-dimensional (2D) profiles of ion concentrations in the nanochannels under +1.5 and −1.5 V in different states. At state "1", when pH = 5, the heterogeneous channel is completely positive, demonstrating anion (mainly Cl^-) selectivity. Since the pore size of MTI is comparable to the thickness of EDL and the porosity is larger compared with AAO, chloride ions preferentially transfer from the MTI side to the AAO side (Figure 5b).[49] The theoretical calculation revealed that a voltage of +1.5 V resulted in a high ion concentration in the nanochannels, which generated a larger ion current. On the contrary, a voltage of −1.5 V caused an ion depletion region, which reduced the ion current significantly, showing that the rectification ratio is greater than 1. On the other hand, when the pH of the electrolyte is 10, the polarity of the nanochannel's surface charge changes from positive to negative. In this case, a concomitant inverted rectification ratio can be observed, which is less than 1.[50] At state "2", light

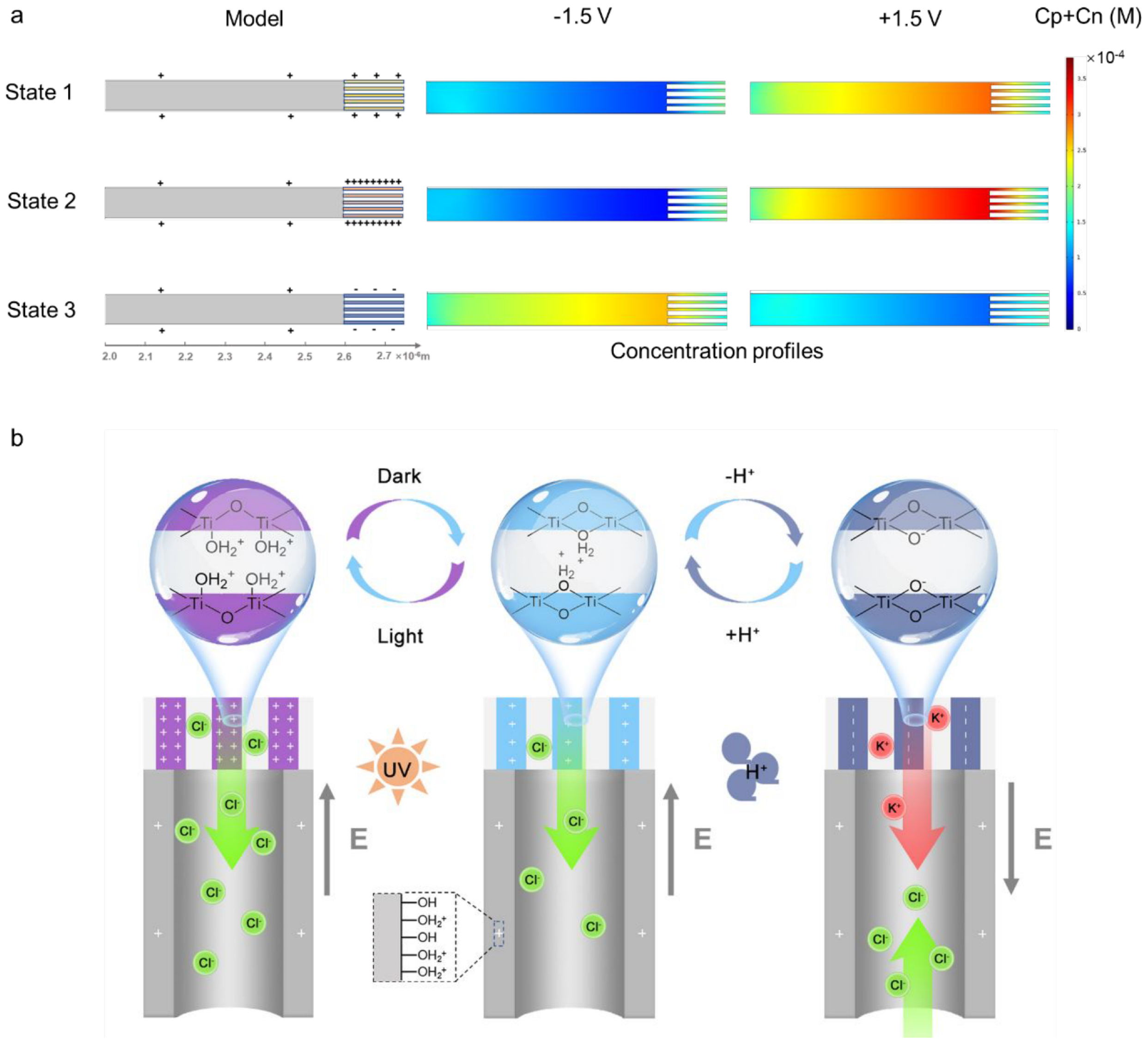

Figure 5. (a) Calculated ion concentration profile inside the MTI/AAO heterogeneous membrane in three states. (b) Ion transport diagram of the MTI/AAO heterogeneous membrane.

promotes the separation of electrons and holes in titanium dioxide, and the surface charge density of titanium dioxide increased due to the increase of hydroxyl groups.[51,52] Therefore, the ion current becomes larger under the illumination. The zeta potential of the MTI increased under light, further proving that light promotes the enhancement of surface charge as shown in Figure S24. As suggested by the 2D profile of the ion concentration, the concentration of the heterogeneous nanochannels under the illumination is higher as compared to that in the dark. Owing to the photoinduced surface charge of the MTI channel, more anions passed through the channel accompanied by higher ion currents leading to a higher rectification ratio. When the pH value of the electrolyte changed to 7.5 (state "3"), the MTI is negatively charged. Meanwhile, the AAO on the other side of the channel is positively charged, forming a charge heterogeneous structure.[53] Therefore, under negative bias, cations are preferentially transported from the MTI side to the AAO side, and anions are transported from the AAO side to the titanium dioxide side, causing ion enrichment. Under the opposite positive bias, the anions and cations are transported in opposite directions, causing ion dissipation and leading to the ion rectification ratio less than 1. These calculation results are consistent with our experimental data.

■ CONCLUSION

In conclusion, a simple and efficient superassembly strategy was developed to fabricate heterogeneous membranes composed of ordered mesoporous titania nanopillar-arrays/alumina oxide (MTI/AAO). These asymmetric multifunctional heterogeneous membranes can integrate a light and pH dual response, improving the sensitivity and selectivity of ion regulation. The photoresponsive current density can reach up to 291.2 μA·cm^{-2}, which has exceeded the existing works. Furthermore, the artificial nanochannels exhibited good reversibility and stability toward alternate illumination based on the surface charge changes within the nanochannels. This heterogeneous membrane can potentially be integrated into intelligent devices for many real-world applications such as biosensing and energy conversion.

■ MATERIALS AND METHODS

Chemicals. Tetraisopropyl orthotitanate (TTIP), concentrated hydrochloric acid (HCl), and ethanol were obtained from Sinopharm Chemical Reagent Co., Ltd. Pluronic P123 [poly(ethylene glycol)−*block*-poly(propylene glycol)−*block*-poly(ethylene glycol)] was purchased from Sigma-Aldrich. All chemicals were used as received without any further purification. Deionized water (18.2 MΩ cm, Milli-Q) was used in the experiments. Potassium chloride (KCl) was obtained from Macklin. An anodic aluminum oxide (AAO) membrane (pore density = 10^{12} cm^{-2}) was purchased from Hefei Pu-Yuan Nanotechnology.

Preparation of the Titanium Precursor Solution. Dilute hydrochloric acid (0.74 g) was slowly added dropwise to 1.05 g of tetraisopropyl orthotitanate (TTIP) and stirred for 10 min at room temperature. P123 colorless transparent gel (0.2 g) was dissolved in 3 g of absolute ethanol, and this solution was slowly added to the dilute hydrochloric acid solution of TTIP and stirred for 15 min at room temperature.

Synthesis of the MTI/AAO Nanochannels. A 60 μm thick AAO film was coated with 10 wt % solution of PMMA in acetone. After that, it was dried at room temperature for 2 h and heated at 200 °C for about 5 h to ensure the PMMA solution could penetrate into the large pore of AAO. The PMMA on the AAO surface was removed by sandpaper. Then, the prepared mesoporous titanium precursor solution was spin-coated on the surface of the AAO at a rate of 3000 rpm for 30 s, followed by aging for 24 h at −20 °C. Afterward, the films were finally calcined using a tube furnace at various temperatures (200−500 °C) for 4 h in air with a ramp rate of 1 °C/min.

Characterization. The microstructure of the film was observed using a Shimadzu S4800 scanning electron microscope, a Hitachi HT-7700 microscope, and a Tecnai G2 F20 S-Twin (high-resolution) field emission transmission electron microscope. The crystalline phase of the templated film was determined using a D/tex-Ultima TV wide-angle X-ray diffractometer (XRD) equipped with Cu Kα radiation. N_2 adsorption−desorption isothermal analysis was carried out using a Quantachrome Quadrasorb evo analyzer at −196 °C. The BET method was utilized to calculate surface areas, and the Barrett−Joyner−Halenda (BJH) model was used to calculate pore size distributions. The zeta potential of the MTI was examined using a zeta potential analyzer (Zetasizer Nano ZS90). UV−vis absorption spectrum of MTI was measured by Lambda 650S.

Electrochemical Measurements. In order to study the ion transport characteristics of MTI/AAO heterogeneous nanochannels, the membranes were installed in an electrochemical cell with a quartz window that was filled with KCl aqueous solution with different pH values and concentrations. The ionic transportation properties of the heterogeneous nanochannels were recorded with a picoammeter (Keithley 6487) using a pair of Ag/AgCl electrodes. The anode was always set on the AAO side, and the cathode was set on the MTI side. The current−time ($I-T$) measurements were performed with 1 mM KCl solution at a pH of 5 under alternating illumination. A solar light simulator (PLS-SXE300/300UV) was used as the light source, with an intensity of approximately 3.5 mW·cm^{-2}. The transmembrane voltage was applied from −1.5 to +1.5 V across the nanochannels during the $I-V$ property measurements. Each test was repeated three times to obtained average ionic current values. All measurements were carried out at room temperature.

Safety Statement. No unexpected or unusually high safety hazards were encountered.

■ ASSOCIATED CONTENT

Supporting Information

The Supporting Information is available free of charge at https://pubs.acs.org/doi/10.1021/acscentsci.1c01402.

> SEM image of pure AAO nanochannels; TGA curve of P123; characterization analysis of photographs, SEM, TEM, and XRD patterns of MTI/AAO heterostructure films prepared at different calcination temperatures; FT-IR spectrum and UV−vis absorption spectrum of MTI; ionic conductance of a heterogeneous membrane under different KCl concentrations in the dark and under illumination; current density−time curves of MTI/AAO under different illumination intensities; current density and voltage change under different illumination intensities; current density generated by water decomposition; current density−time curves of heterogeneous MTI/AAO heterogeneous nanochannels under alternating illumination in different UV wavelengths; isoelectric point of MTI; ion current rectification ratio of MTI/AAO heterogeneous nanochannels calcined at 350 °C; $I-V$ curves of MTI/AAO with different apertures before and after illumination; numerical simulation model of the MTI/AAO heterogeneous membrane; zeta potential of MTI in darkness and light; comparison with the previously reported light-responsive nanochannel (PDF)

■ AUTHOR INFORMATION

Corresponding Author

Biao Kong − *Department of Chemistry, Shanghai Key Lab of Molecular Catalysis and Innovative Materials and Collaborative Innovation Center of Chemistry for Energy Materials, Fudan University, Shanghai 200438, P. R. China;* orcid.org/0000-0002-3251-5071; Email: bkong@fudan.edu.cn

Authors

Xin Zhang − *Department of Chemistry, Shanghai Key Lab of Molecular Catalysis and Innovative Materials and Collaborative Innovation Center of Chemistry for Energy Materials, Fudan University, Shanghai 200438, P. R. China*

Lei Xie − *Department of Chemistry, Shanghai Key Lab of Molecular Catalysis and Innovative Materials and Collaborative Innovation Center of Chemistry for Energy Materials, Fudan University, Shanghai 200438, P. R. China;* orcid.org/0000-0003-4751-4271

Shan Zhou − *Department of Chemistry, Shanghai Key Lab of Molecular Catalysis and Innovative Materials and Collaborative Innovation Center of Chemistry for Energy Materials, Fudan University, Shanghai 200438, P. R. China*

Hui Zeng − *Department of Chemistry, Shanghai Key Lab of Molecular Catalysis and Innovative Materials and Collaborative Innovation Center of Chemistry for Energy Materials, Fudan University, Shanghai 200438, P. R. China*

Jie Zeng − *Department of Chemistry, Shanghai Key Lab of Molecular Catalysis and Innovative Materials and Collaborative Innovation Center of Chemistry for Energy Materials, Fudan University, Shanghai 200438, P. R. China*

Tianyi Liu − *Department of Chemistry, Shanghai Key Lab of Molecular Catalysis and Innovative Materials and Collaborative Innovation Center of Chemistry for Energy Materials, Fudan University, Shanghai 200438, P. R. China*

Qirui Liang − *Department of Chemistry, Shanghai Key Lab of Molecular Catalysis and Innovative Materials and Collaborative Innovation Center of Chemistry for Energy Materials, Fudan University, Shanghai 200438, P. R. China*

Miao Yan − *Department of Chemistry, Shanghai Key Lab of Molecular Catalysis and Innovative Materials and Collaborative Innovation Center of Chemistry for Energy Materials, Fudan University, Shanghai 200438, P. R. China;* orcid.org/0000-0002-0546-6630

Yanjun He − *Department of Chemistry, Shanghai Key Lab of Molecular Catalysis and Innovative Materials and Collaborative Innovation Center of Chemistry for Energy Materials, Fudan University, Shanghai 200438, P. R. China*

Kang Liang − *School of Chemical Engineering and Graduate School of Biomedical Engineering, The University of New South Wales, Sydney, NSW 2052, Australia;* orcid.org/0000-0003-3985-7688

Lei Zhang − *Department of Chemical Engineering, University of Waterloo, Waterloo, Ontario N2L 3G1, Canada;* orcid.org/0000-0001-5454-8758

Pu Chen − *Department of Chemical Engineering, University of Waterloo, Waterloo, Ontario N2L 3G1, Canada;* orcid.org/0000-0002-6706-8291

Lei Jiang − *Laboratory of Bio-inspired Materials and Interfacial Science, Technical Institute of Physics and Chemistry, Chinese Academy of Sciences, Beijing 100190, P.R. China;* orcid.org/0000-0003-4579-728X

Complete contact information is available at: https://pubs.acs.org/10.1021/acscentsci.1c01402

Notes

The authors declare no competing financial interest.

■ ACKNOWLEDGMENTS

This work was supported by the National Key Research and Development Program of China (2019YFC1604601, 2019YFC1604600, 2017YFA0206901, 2017YFA0206900, 2018YFC1602301), the National Natural Science Foundation of China (21705027, 21974029, 2210050428), the Natural Science Foundation of Shanghai (18ZR1404700), and the Construction Project of Shanghai Key Laboratory of Molecular Imaging (18DZ2260400), Shanghai Municipal Education Commission (Class II Plateau Disciplinary Construction Program of Medical Technology of SUMHS, 2018-2020). We gratefully acknowledge Professor Dongyuan Zhao at Fudan University for valuable advice.

■ REFERENCES

(1) Gadsby, D. C. Ion channels versus ion pumps: the principal difference, in principle. *Nat. Rev. Mol. Cell Biol.* **2009**, *10*, 344−352.

(2) Zhang, Z.; Kong, X.-Y.; Xiao, K.; Liu, Q.; Xie, G.; Li, P.; Ma, J.; Tian, Y.; Wen, L.; Jiang, L. Engineered Asymmetric Heterogeneous Membrane: A Concentration-Gradient-Driven Energy Harvesting Device. *J. Am. Chem. Soc.* **2015**, *137*, 14765−14772.

(3) Zhang, Z.; Sui, X.; Li, P.; Xie, G.; Kong, X.-Y.; Xiao, K.; Gao, L.; Wen, L.; Jiang, L. Ultrathin and Ion-Selective Janus Membranes for High-Performance Osmotic Energy Conversion. *J. Am. Chem. Soc.* **2017**, *139*, 8905−8914.

(4) Xie, L.; Zhou, S.; Liu, J.; Qiu, B.; Liu, T.; Liang, Q.; Zheng, X.; Li, B.; Zeng, J.; Yan, M.; He, Y.; Zhang, X.; Zeng, H.; Ma, D.; Chen, P.; Liang, K.; Jiang, L.; Wang, Y.; Zhao, D.; Kong, B. Sequential Superassembly of Nanofiber Arrays to Carbonaceous Ordered Mesoporous Nanowires and Their Heterostructure Membranes for Osmotic Energy Conversion. *J. Am. Chem. Soc.* **2021**, *143*, 6922−6932.

(5) Zhang, L.; Zhou, S.; Xie, L.; Wen, L.; Tang, J.; Liang, K.; Kong, X.; Zeng, J.; Zhang, R.; Liu, J.; Qiu, B.; Jiang, L.; Kong, B. Interfacial Super-Assembly of T-Mode Janus Porous Heterochannels from Layered Graphene and Aluminum Oxide Array for Smart Oriented Ion Transportation. *Small* **2021**, *17*, 2100141.

(6) Zhou, S.; Zhang, L.; Xie, L.; Zeng, J.; Qiu, B.; Yan, M.; Liang, Q.; Liu, T.; Liang, K.; Chen, P.; Kong, B. Interfacial Super-Assembly of Nanofluidic Heterochannels from Layered Graphene and Alumina Oxide Arrays for Label-Free Histamine-Specific Detection. *Anal. Chem.* **2021**, *93*, 2982−2987.

(7) Zhou, S.; Xie, L.; Li, X.; Huang, Y.; Zhang, L.; Liang, Q.; Yan, M.; Zeng, J.; Qiu, B.; Liu, T.; Tang, J.; Wen, L.; Jiang, L.; Kong, B. Interfacial Super-Assembly of Ordered Mesoporous CarbonSilica/AAO Hybrid Membrane with Enhanced Permselectivity for Temperature- and pH-Regulated Smart Ion Transport. *Angew. Chem., Int. Ed.* **2021**, *60*, 26167−26176.

(8) Wang, C.; Liu, F.-F.; Tan, Z.; Chen, Y.-M.; Hu, W.-C.; Xia, X.-H. Fabrication of Bio-Inspired 2D MOFs/PAA Hybrid Membrane for Asymmetric Ion Transport. *Adv. Funct. Mater.* **2020**, *30*, 1908804.

(9) Lv, Y.; Yang, N.; Lu, S.; Xiang, Y. Ion Transport of Biohybrid Asymmetric Membranes by pH and Light-Cooperative Modulation. *Adv. Mater. Interfaces* **2020**, *7*, 2001134.

(10) Wu, Y.-Y.; Chen, L.-D.; Cai, X.-H.; Zhao, Y.; Chen, M.; Pan, X.-H.; Li, Y.-Q. Smart pH-Modulated Two-Way Photoswitch Based on a Polymer-Modified Single Nanochannel. *ACS Appl. Mater. Interfaces* **2021**, *13*, 25241−25249.

(11) Siwy, Z. S.; Howorka, S. Engineered voltage-responsive nanopores. *Chem. Soc. Rev.* **2010**, *39*, 1115−1132.

(12) Bao, B.; Hao, J.; Bian, X.; Zhu, X.; Xiao, K.; Liao, J.; Zhou, J.; Zhou, Y.; Jiang, L. 3D Porous Hydrogel/Conducting Polymer Heterogeneous Membranes with Electro-/pH-Modulated Ionic Rectification. *Adv. Mater.* **2017**, *29*, 1702926.

(13) Wu, M.-Y.; Li, Z.-Q.; Zhu, G.-L.; Wu, Z.-Q.; Ding, X.-L.; Huang, L.-Q.; Mo, R.-J.; Xia, X.-H. Electrochemically Switchable Double-Gate Nanofluidic Logic Device as Biomimetic Ion Pumps. *ACS Appl. Mater. Interfaces* **2021**, *13*, 32479−32485.

(14) Yameen, B.; Ali, M.; Neumann, R.; Ensinger, W.; Knoll, W.; Azzaroni, O. Ionic transport through single solid-state nanopores controlled with thermally nanoactuated macromolecular gates. *Small* **2009**, *5*, 1287−1291.

(15) Zhang, Z.; Xie, G.; Xiao, K.; Kong, X.-Y.; Li, P.; Tian, Y.; Wen, L.; Jiang, L. Asymmetric Multifunctional Heterogeneous Membranes for pH- and Temperature-Cooperative Smart Ion Transport Modulation. *Adv. Mater.* **2016**, *28*, 9613−9619.

(16) Liu, J.; Wang, N.; Yu, L.-J.; Karton, A.; Li, W.; Zhang, W.; Guo, F.; Hou, L.; Cheng, Q.; Jiang, L.; Weitz, D. A.; Zhao, Y. Bioinspired graphene membrane with temperature tunable channels for water gating and molecular separation. *Nat. Commun.* **2017**, *8*, 2011.

(17) Chen, K.; Yao, L.; Su, B. Bionic Thermoelectric Response with Nanochannels. *J. Am. Chem. Soc.* **2019**, *141*, 8608−8615.

(18) Chen, K.; Yao, L.; Yan, F.; Liu, S.; Yang, R.; Su, B. Thermo-osmotic energy conversion and storage by nanochannels. *J. Mater. Chem. A* **2019**, *7*, 25258−25261.

(19) Xiao, K.; Xie, G.; Li, P.; Liu, Q.; Hou, G.; Zhang, Z.; Ma, J.; Tian, Y.; Wen, L.; Jiang, L. A Biomimetic Multi-Stimuli-Response Ionic Gate Using a Hydroxypyrene Derivation-Functionalized Asymmetric Single Nanochannel. *Adv. Mater.* **2014**, *26*, 6560−6565.

(20) Zhang, Q.; Liu, Z.; Wang, K.; Zhai, J. Organic/Inorganic Hybrid Nanochannels Based on Polypyrrole-Embedded Alumina Nanopore Arrays: pH- and Light-Modulated Ion Transport. *Adv. Funct. Mater.* **2015**, *25*, 2091−2098.

(21) Li, R.; Sui, X.; Li, C.; Jiang, J.; Zhai, J.; Gao, L. Artificial NO and Light Cooperative Nanofluidic Diode Inspired by Stomatal Closure of Guard Cells. *ACS Appl. Mater. Interfaces* **2018**, *10*, 3241−3247.

(22) Xiao, K.; Chen, L.; Chen, R.; Heil, T.; Lemus, S. D. C.; Fan, F.; Wen, L.; Jiang, L.; Antonietti, M. Artificial light-driven ion pump for photoelectric energy conversion. *Nat. Commun.* **2019**, *10*, 74.

(23) Liu, J.; Fu, B.; Zhang, Z. Ionic Current Rectification Triggered Photoelectrochemical Chiral Sensing Platform for Recognition of Amino Acid Enantiomers on Self-Standing Nanochannel Arrays. *Anal. Chem.* **2020**, *92*, 8670−8674.

(24) Zhao, C.; Wang, H.; Zhang, H. Bio-inspired artificial ion channels: from physicalto chemical gating. *Mater. Chem. Front.* **2021**, *5*, 4059−4072.

(25) Xiao, K.; Giusto, P.; Chen, F.; Chen, R.; Heil, T.; Cao, S.; Chen, L.; Fan, F.; Jiang, L. Light-driven directional ion transport for enhanced osmotic energy harvesting. *Natl. Sci. Rev.* **2021**, *8*, nwaa231.

(26) Fu, L.; Zhai, J. Biomimetic stimuli-responsive nanochannels and their applications. *Electrophoresis* **2019**, *40*, 2058−2074.

(27) Zhang, D.; Ren, Y.; Fan, X.; Zhai, J.; Jiang, L. Photoassisted salt-concentration-biased electricity generation using cation-selective porphyrin-based nanochannels membrane. *Nano Energy* **2020**, *76*, 105086.

(28) Cai, J.; Ma, W.; Hao, C.; Sun, M.; Guo, J.; Xu, L.; Xu, C.; Kuang, H. Artificial light-triggered smart nanochannels relying on optoionic effects. *Chem.* **2021**, *7*, 1802−1826.

(29) Hu, Z.; Zhang, Q.; Gao, J.; Liu, Z.; Zhai, J.; Jiang, L. Photocatalysis-triggered ion rectification in artificial nanochannels based on chemically modified asymmetric TiO_2 nanotubes. *Langmuir* **2013**, *29*, 4806−4812.

(30) Ren, H.; Xiao, T.; Zhang, Q.; Liu, Z. Photosynthesis-inspired bifunctional energy-harvesting devices that convert light and salinity gradients into electricity. *Chem. Commun.* **2018**, *54*, 12310−12313.

(31) Yang, X.; Qiu, P.; Yang, J.; Fan, Y.; Wang, L.; Jiang, W.; Cheng, X.; Deng, Y.; Luo, W. Mesoporous Materials-Based Electrochemical Biosensors from Enzymatic to Nonenzymatic. *Small* **2021**, *17*, 1904022.

(32) Zhang, Q.; Liu, Z.; Zhai, J. Photocurrent generation in a light-harvesting system with multifunctional artificial nanochannels. *Chem. Commun.* **2015**, *51*, 12286−12289.

(33) Zhang, Q.; Hu, Z.; Liu, Z.; Zhai, J.; Jiang, L. Light-Gating Titania/Alumina Heterogeneous Nanochannels with Regulatable Ion Rectification Characteristic. *Adv. Funct. Mater.* **2014**, *24*, 424−431.

(34) Zhou, S.; Xie, L.; Zhang, L.; Wen, L.; Tang, J.; Zeng, J.; Liu, T.; Peng, D.; Yan, M.; Qiu, B.; Liang, Q.; Liang, K.; Jiang, L.; Kong, B. Interfacial Super-Assembly of Ordered Mesoporous Silica-Alumina Heterostructure Membranes with pH-Sensitive Properties for Osmotic Energy Harvesting. *ACS Appl. Mater. Interfaces* **2021**, *13*, 8782−8793.

(35) Foong, T. R. B.; Shen, Y.; Hu, X.; Sellinger, A. Template-Directed Liquid ALD Growth of TiO_2 Nanotube Arrays: Properties and Potential in Photovoltaic Devices. *Adv. Funct. Mater.* **2010**, *20*, 1390−1396.

(36) Zhao, D.; Feng, J.; Huo, Q.; Melosh, N.; Fredrickson, G. H.; Chmelka, B. F.; Stucky, G. D. *Science* **1998**, *279*, 548−552.

(37) Wu, C.-W.; Ohsuna, T.; Kuwabara, M.; Kuroda, K. Formation of Highly Ordered Mesoporous Titania Films Consisting of Crystalline Nanopillars with Inverse Mesospace by Structural Transformation. *J. Am. Chem. Soc.* **2006**, *128*, 4544−4545.

(38) Uchida, H.; Patel, M. N.; May, R. A.; Gupta, G.; Stevenson, K. J.; Johnston, K. P. Highly-ordered mesoporous titania thin films prepared via surfactant assembly on conductive indium−tin-oxide/glass substrate and its optical properties. *Thin Solid Films* **2010**, *518*, 3169−3176.

(39) Malgras, V.; Shirai, Y.; Takei, T.; Yamauchi, Y. Coalescence-Driven Verticality in Mesoporous TiO_2 Thin Films with Long-Range Ordering. *J. Am. Chem. Soc.* **2020**, *142*, 15815−15822.

(40) Choi, S. Y.; Lee, B.; Carew, D. B.; Mamak, M.; Peiris, F. C.; Speakman, S.; Chopra, N.; Ozin, G. A. 3D Hexagonal (R-3m) Mesostructured Nanocrystalline Titania Thin Films: Synthesis and Characterization. *Adv. Funct. Mater.* **2006**, *16*, 1731−1738.

(41) Mahoney, L.; Koodali, R. T. Versatility of Evaporation-Induced Self-Assembly (EISA) Method for Preparation of Mesoporous TiO_2 for Energy and Environmental Applications. *Materials* **2014**, *7*, 2697−2746.

(42) Li, W.; Liang, R.; Hu, A.; Huang, Z.; Zhou, Y.-N. Generation of oxygen vacancies in visible light activated one-dimensional iodine TiO_2 photocatalysts. *RSC Adv.* **2014**, *4*, 36959−36966.

(43) Guayaquil-Sosa, J. F.; Serrano-Rosales, B.; Valadés-Pelayo, P. J.; de Lasa, H. Photocatalytic hydrogen production using mesoporous TiO_2 doped with Pt. *Applied Catalysis B: Environmental* **2017**, *211*, 337−348.

(44) Stein, D.; Kruithof, M.; Dekker, C. Surface-charge-governed ion transport in nanofluidic channels. *Phys. Rev. Lett.* **2004**, *93*, 035901.

(45) Tsuchiya, H.; Macak, J. M.; Ghicov, A.; Räder, A. S.; Taveira, L.; Schmuki, P. Characterization of electronic properties of TiO_2 nanotube films. *Corros. Sci.* **2007**, *49*, 203−210.

(46) Yan, R.; Liang, W.; Fan, R.; Yang, P. Nanofluidic Diodes Based on NanotubeHeterojunctions. *Nano Lett.* **2009**, *9*, 3820−3825.

(47) Bohinc, K.; Kralj-Iglic, V.; Iglic, A. Thickness of electrical double layer. Effect of ion size. *Electrochim. Acta* **2001**, *46*, 3033−3040.

(48) Zhang, Q.; Liu, Z.; Hou, X.; Fan, X.; Zhai, J.; Jiang, L. Light-regulated ion transport through artificial ion channels based on TiO_2 nanotubular arrays. *Chem. Commun.* **2012**, *48*, 5901−5903.

(49) Gao, J.; Guo, W.; Feng, D.; Wang, H.-T.; Zhao, D.-Y.; Jiang, L. High-Performance Ionic Diode Membrane for Salinity Gradient Power Generation. *J. Am. Chem. Soc.* **2014**, *136*, 12265−12272.

(50) Umehara, S.; Pourmand, N.; Webb, C. D.; Davis, R. W.; Yasuda, K.; Karhanek, M. Current Rectification with Poly-L-Lysine-Coated Quartz Nanopipettes. *Nano Lett.* **2006**, *6*, 2486−2492.

(51) Fujishima, A.; Rao, T. N.; Tryk, D. A. Titanium dioxide photocatalysis. *J. Photoch. Photobio. C* **2000**, *1*, 1−21.

(52) Sakai, N.; Fujishima, A.; Watanabe, T.; Hashimoto, K. Quantitative evaluation of the photoinduced hydrophilic conversion properties of TiO_2 thin film surfaces by the reciprocal of contact angle. *J. Phys. Chem. B* **2003**, *107*, 1028−1035.

(53) Daiguji, H.; Oka, Y.; Shirono, K. Nanofluidic diode and bipolar transistor. *Nano Lett.* **2005**, *5*, 2274−2280.